JPL Publication 96-19

Objective Interpolation of Scatterometer Winds

Wenqing Tang
W. Timothy Liu

August 1, 1996

National Aeronautics and
Space Administration

Jet Propulsion Laboratory
California Institute of Technology
Pasadena, California

The study described in this publication was carried out by the Jet Propulsion Laboratory, California Institute of Technology, under a contract with the National Aeronautics and Space Administration (NASA). It was jointly supported by the NASA Scatterometer Project and the Physical Oceanography Program of the Mission to Planet Earth.

Abstract

Global wind fields are produced by successive corrections that use measurements by the European Remote Sensing Satellite (ERS-1) scatterometer. The methodology is described. The wind fields at 10-meter height provided by the European Center for Medium-Range Weather Forecasting (ECMWF) are used to initialize the interpolation process. The interpolated wind field product ERSI is evaluated in terms of its improvement over the initial guess field (ECMWF) and the bin-averaged ERS-1 wind field (ERSB). Spatial and temporal differences between ERSI, ECMWF and ERSB are presented and discussed.

Table of Contents

1. Introduction

Microwave scatterometers are designed to measure ocean surface wind vectors in both clear and cloudy conditions. Spaceborne scatterometers are the only potential means of measuring ocean surface wind forcing at adequate temporal and spatial scales. The wind shear at the surface represents the momentum exchange that couples the ocean with the atmosphere. The scatterometer on the European satellite ERS-1 has provided ocean surface wind vectors since the summer of 1991 [Attema, 1991].

The application of scatterometer winds in conjunction with atmospheric and oceanic models requires the interpolation of the scatterometer winds to regular latitude-longitude grids at regular time intervals. A scatterometer with limited swath width on a polar orbiter produces irregular spatial and temporal coverage, and the difficulties in producing wind maps in such a case have been discussed using simulated data [e.g., Kelly and Caruso, 1990; Zeng and Levy, 1995]. Unlike its predecessor on Seasat, which scanned on both sides of the spacecraft, the scatterometer on ERS-1 scans only on one side of the spacecraft, producing a 475-km swath and leaving large data gaps between orbits. The problem of interpolation is obvious from Fig.1, which shows the coverage in a typical 12-hour period.

This is a report on the 1° latitude by 1° longitude, 12-hour wind vector maps generated by interpolation of ERS-1 scatterometer data from successive corrections. The interpolated wind fields have been applied to study the relation between intraseasonal wind burst and anomalous equatorial warming [Liu et al., 1995], monsoon onset and wind-driven surface current [Liu and Tang, 1996], the intensity and location of typhoons [Hsu and Liu, 1996], and tropical convection and hydrologic balance [Hsu et al.,1996].

In this report, the methodology of interpolation is described in Section 2, and the interpolation is evaluated in terms of its improvement over the initial guess field and the bin-averaged wind field in Section 3. The wind vectors were retrieved from scatterometer observations by using the model function developed by Freilich and Dunbar [1993]. The accuracy of wind vectors retrieved by various model functions is being vigorously tested by a number of investigators and is beyond the scope of this report.

2. The Successive Corrections Scheme

The objective analysis of ERS-1 scatterometer observations described in this report was accomplished by the method of successive corrections, proposed by Bergthorsson and Döös [1955] and modified by Cressman [1959]. The interpolation scheme starts from an initial guess field (ug,vg) on the grid, then uses scatterometer observations around the grid point within the influence radius of space R_n and time T_d, to iteratively correct the value of (ug,vg). The contributions of observations to the correction term are weighted differently based on their positions relative to the grid point under analysis. The procedure was applied to zonal and meridional wind components separately. Every twelve hours, at 0Z and 12Z, a synoptic field is produced on a grid of 1°x1° resolution; it covers an area from 60°S to 60°N latitudinally and is global longitudinally.

The guess value for the wind vector on grid point (i,j) at the n-th iteration is denoted by ($ug_{i,j}^n$, $vg_{i,j}^n$). All the equations in this section are expressed in terms of $ug_{i,j}^n$ only. The corresponding equations for $vg_{i,j}^n$ can be similarly derived. The key point for the successive corrections is embedded in the equation

$$ug_{i,j}^{n+1} = ug_{i,j}^n + \gamma C_{i,j}^n \qquad (1)$$

where γ is a weighting factor and $C_{i,j}^n$ is the correction term representing the impact from the observations, in this case, the impact from the ERS-1 scatterometer measurements. To produce a map of a particular time T, the value on each grid point is initialized by ECMWF winds at T. The ECMWF/TOGA (Tropical Ocean and Global Atmosphere) Level III Data Set contains wind vectors at 10 meters on a 2.5° latitude by 2.5° longitude grid at 0Z and 12Z. A bilinear interpolation scheme is used to interpolate the ECMWF data to a 1°x1° grid. Then all scatterometer observations within the influence time T_d from T are used to correct successively the value on grid points. Since the ERS-1 scatterometer covers the global ocean in about three days, T_d was chosen to be 1.5 days; i.e., a total of 3 days of scatterometer data, one and one-half days before and after T, respectively, are used to produce a map of time T. Scatterometer measurements are screened during the iteration process, on the basis of error criteria explained below.

To figure out the correction term on the n-th iteration, guess fields $ug_{i,j}^n$ were used to calculate the guess field value ug_s^n at location "s" where ERS-1 scatterometer data were obtained. The interpolated guess field value ug_s^n is given by the 9-point Lagrangian interpolation formula:

$$ug_s^n = \sum_{i=I-1,\ j=J-1}^{i=I+1,\ j=J+1} w_{i,j}\ ug_{i,j}^n \qquad (2)$$

where (I,J) is the grid point closest to location "s" and $w_{i,j}$ is the weighting function given by

$$w_{i,j} = \prod_{\substack{k=I-1 \\ k\neq I}}^{k=I+1} \frac{(x - x_k)}{(x_I - x_k)} \qquad \prod_{\substack{l=J-1 \\ l\neq J}}^{l=J+1} \frac{(y - y_l)}{(y_J - y_l)} \qquad (3)$$

Here (x,y) represents the coordinates of location "s".

Next the error E_s^n, the difference between the actual measured scatterometer value u_s at location "s" and the guess value interpolated from the analyzed field at the same location, is computed:

$$E_s^n = u_s - ug_s^n \qquad (4)$$

Observed data were rejected if this error value exceeded the maximum allowable error (E_{max}) as given

in Table I. This error limit is a decreasing function of iteration passes, allowing increasing confidence in the analyzed field with each successive iteration.

The error function E_s^n is used to correct the guess field value on grid points for the (n+1) -th iteration. The correction term is given by

$$C_{i,j}^n = \frac{\Sigma_s W_s^n E_s^n}{\Sigma_s W_s^n} \qquad (5)$$

where the summation is over all observations within the radius of influence, R_n, from grid point (i,j). The value of R_n for each iteration is given in Table I. W_s^n is a weighting function defined as

$$W_s^n = w^n(d)\ \beta(t) \qquad (6)$$

The first factor, $w^n(d)$, signifies weighting of the spatial distance between observed and analyzed points and is a Cressman weighting function [Cressman, 1959]. The second factor, $\beta(t)$, is weighting of the temporal difference between the measurement time and the time for which the synoptic field is produced.

For each wind map, the correction process was performed four times successively. The gridded data were smoothed after the last iteration. So far, three years of ERS scatterometer interpolated wind fields have been produced, for January 1992 to December 1994. JPL supercomputers were used to accomplish the computationally intensive task. As mentioned in Section 1, this unprecedented product, synoptic global wind fields for complete annual cycles, has been applied in several research activities involving scatterometer winds.

3. Evaluation of the Interpolation Method

3a. The Interpolated Wind Field Maps

Two instances of the synoptic global mapping of ocean surface winds provided by the interpolated wind fields are shown in Figs.2a and 2b as examples. They show atmospheric circulation at 12Z for a typical day in boreal summer and winter, respectively. The streamline indicates wind direction, and the color in the images represents wind speed. Major textbook features of atmospheric circulation, for example, the surface convergence at the Intertropical Convergence Zone, or ITCZ; the Trade Winds; the surface divergence at the Horse Latitudes; the mid-latitude cyclones; and the strong winds of the Roaring Forties, are clearly visualized. The global seasonal changes are also obvious in comparing the two figures, with stronger winds in the winter hemisphere in general.

The most common way of producing wind maps is by simple averaging of all data within the space/time grid. In this case, the scatterometer winds were binned and averaged in 1° latitude by 1° longitude boxes every five days, and then were averaged to form monthly means. The monthly zonal and meridional components of the interpolated wind field (ERSI), the initial guess field (ECMWF),

and the monthly bin-averaged scatterometer winds (ERSB) for a typical month are compared in Fig. 3. The differences among these three wind fields are discussed below.

3b. Changes From the Initial Guess Field

There are significant differences between the ERSI and the initial guess, or ECMWF, wind fields. Two features in the differences persist through the seasonal cycles (Fig. 4) and through the three years of data examined. Negative differences in the meridional component are found just north of the equator in all three oceans: the Pacific, Atlantic and Indian. In these areas, the Trade Winds converge and the meridional component changes sign at the ITCZ. The negative differences reflect the different locations of the ITCZ, with a more southern location represented by the ERSI than the ECMWF winds. Over the southern ocean (40°S - 50°S), the Roaring Forties blow from west to east. The differences in the zonal component are largely negative, indicating that ERSI winds are weaker than ECMWF winds. In the mid-latitude North Pacific and North Atlantic, similar negative differences in the zonal components are found, though they are less persistent than in the southern ocean. Over these mid-latitude storm tracks, the high spatial resolution of the scatterometer may provide more accurate locations of storm centers.

3c. Improvement Over the Binned Average

In Fig. 5, the differences between ERSI and ERSB show north-south structures similar to the ground tracks of the satellite. They result from undersampling by the ERS-1 scatterometer, as reported by Zeng and Levy [1995]. Fig. 3 shows that objective interpolation clearly eliminates most of these track-oriented errors.

3d. Temporal Variance

The power spectra for the three data sets are compared in Fig.6, as an example, for four locations in the Pacific. For each grid point, the power spectrum is calculated using one year of data, with 730 points for ERSI and ECMWF, but 73 points for ERSB. Only the spectra for 1993 are shown; they are almost identical to those for the other two years of data. The binned data show significantly lower energy everywhere at all frequencies. At frequencies higher than one cycle per a few days, ERSI winds appear to have lower energy than ECMWF winds, particularly in the tropical and subtropical oceans, reflecting the poor sampling of the ERS-1 scatterometer. In the data-sparse southern ocean, the interpolated ERS-1 data show significantly more energy than the ECMWF data at frequencies lower than one cycle per 3 to 5 days, indicating that the spaceborne sensor observed more variability than is exhibited by the sparse data assimilated in the numerical weather prediction model.

4. Future Potential for Scatterometer Winds

The NASA scatterometer (NSCAT) will be launched in August 1996 on the Japanese spacecraft ADEOS-1. It will scan two 600-km swaths, one on each side of the spacecraft, and will have more than twice the coverage of the ERS scatterometers. Interpolation methods, with and without the operational numerical weather prediction wind field as an initial guess, are being explored. Both ERS-2 scatterometer winds and winds derived from the Special Sensor Microwave Imager

(SSMI) will be available at the same time as the NSCAT winds, providing unprecedented potential to construct ocean surface wind fields.

5. References

Attema, E.P.W., 1991: The active microwave instrument on board the ERS-1 satellite. Proc. IEEE, 79, 791-799.

Bergthorsson, P., and B. R. Döös, 1955: Numerical weather map analysis. Tellus 7, 329-340.

Cressman, G. P., 1959: An operational objective analysis system. *Mon. Wea. Rev. 87*, 367-374.

Hsu, C. S., and W.T. Liu, 1996: Wind and pressure fields near Tropical Cyclone Oliver derived from scatterometer observations. J. Geophys. Res., accepted.

Hsu, C.S., W.T. Liu, and M.G. Wurtele, 1996: Impact of scatterometer winds on hydrologic forcing and convective heating through surface divergence. Mon. Wea. Rev., accepted.

Freilich, M.H., and R.S. Dunbar, 1993: A preliminary C-band scatterometer model function for the ERS-1 AMI instrument. Proc. First ERS-1 Symp., ESA SP-359, 79-83.

Kelly, K., and M.J. Caruso, 1990: A modified objective mapping technique of scatterometer wind data. J. Geophys. Res., 95, 13,483-13,496.

Liu, W.T., W. Tang, and L.L. Fu, 1995: Recent Warming Event in the Pacific May Be an El Nino. Eos, Trans. of Amer. Geophys. Union, 76, No. 43, 429, 437.

Liu, W.T., and W. Tang, 1996: Spaceborne scatterometer in studies of atmospheric and oceanic phenomena from synoptic to interannual time scales. Space Remote Sensing of Subtropical Ocean. C.T. Liu (ed.), Elsevier Press, Amsterdam, in press.

Zeng, L., and G. Levy, 1995: Space and time aliasing structure in monthly mean polar-orbiting satellite data. J. Geophys. Res., 100, 5133-5142.

Table I. Parameters used in successive corrections

Parameters	Iteration Pass 1	Pass 2	Pass 3	Pass 4
R_n (unit of grid space)	10	6	4	2
E_{max} (m/s)	30	10	5	3

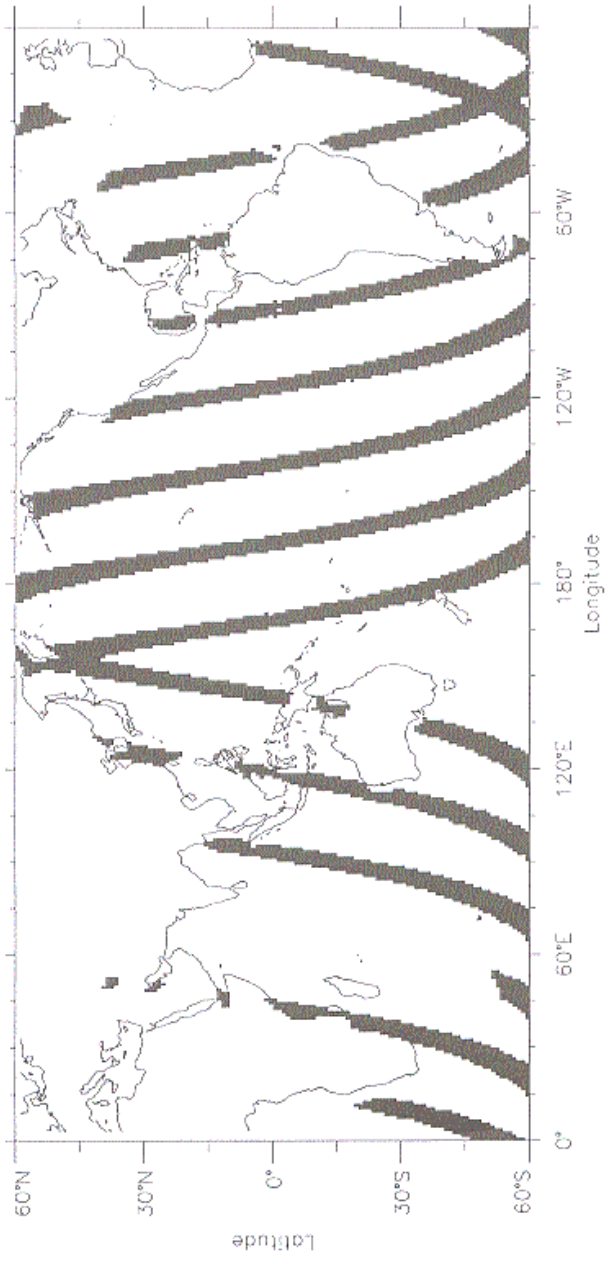

Fig.1. ERS-1 scatterometer coverage in a 12-hour period (black swath).

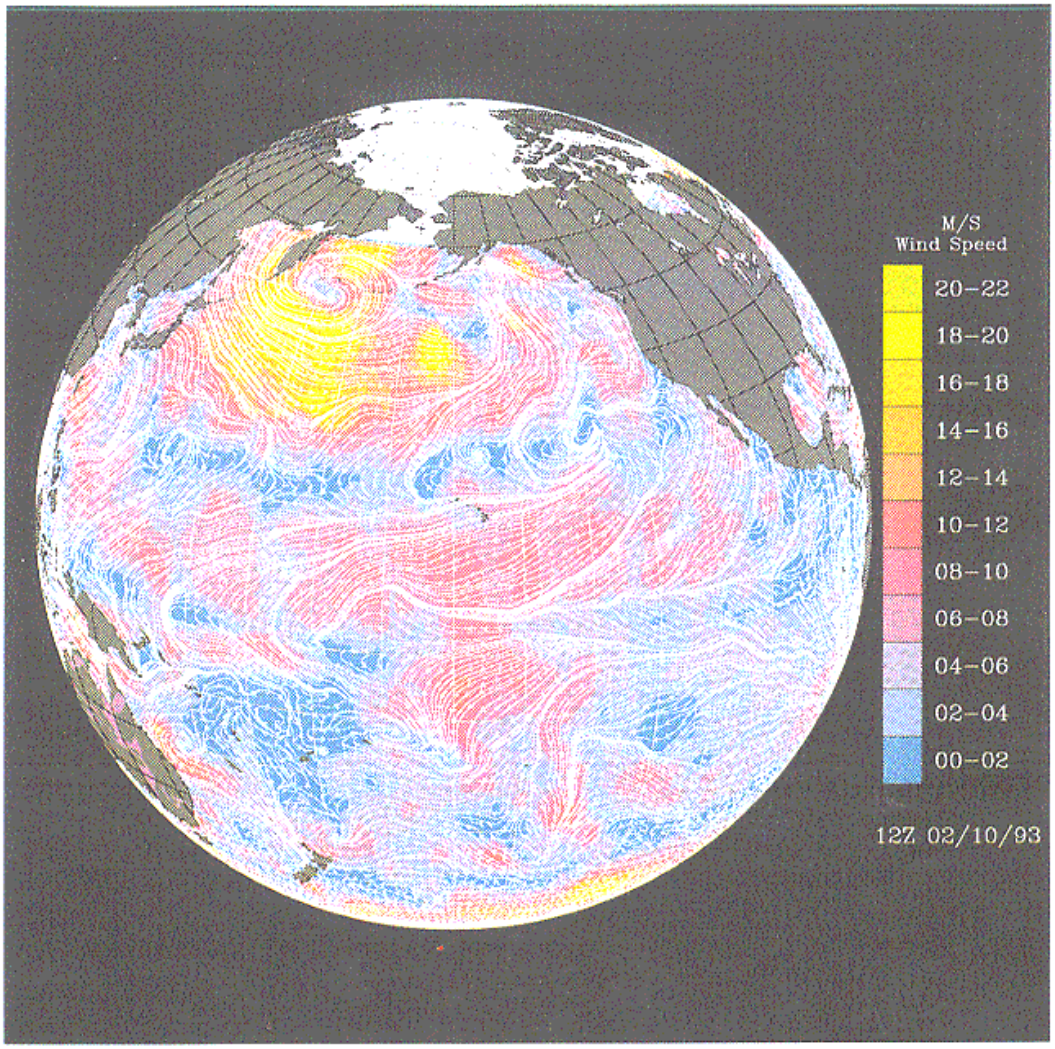

Fig.2a. Synoptic wind field derived from interpolated ERS-1 scatterometer data for February 10, 1993. Color in the image represents wind speed, and the streamline indicates wind direction.

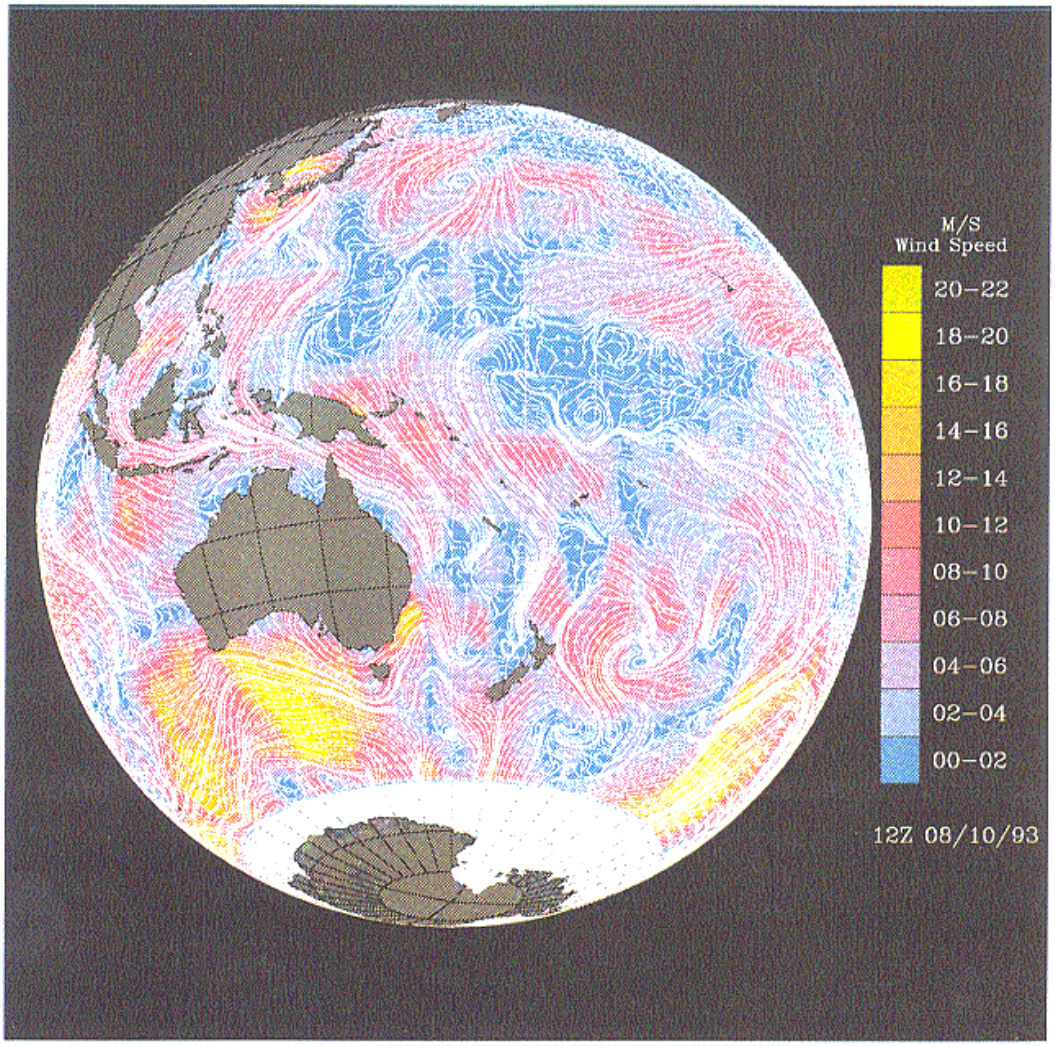

Fig.2b. Synoptic wind field derived from interpolated ERS-1 scatterometer data for August 10, 1993. Color in the image represents wind speed, and the streamline indicates wind direction.

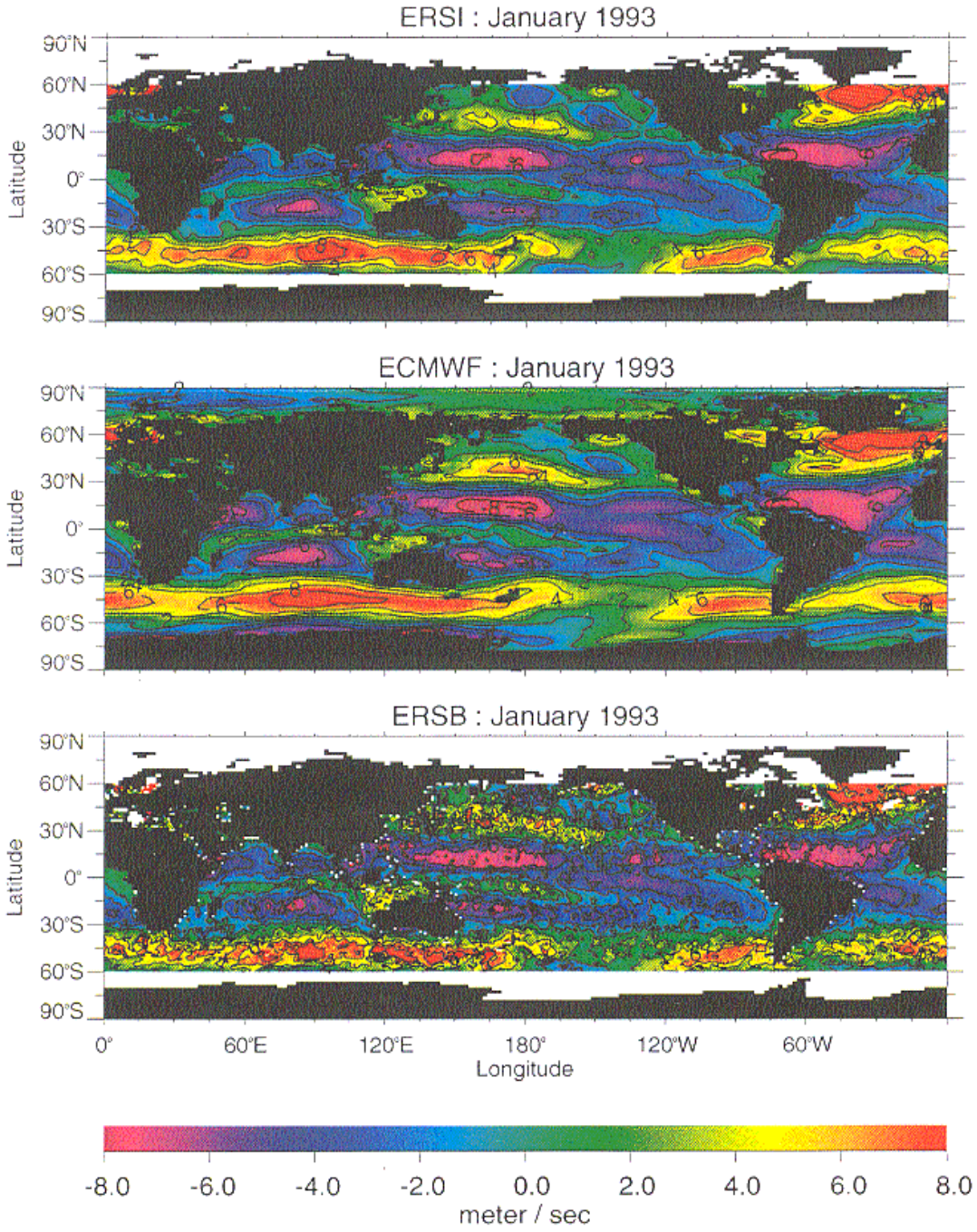

Fig.3a. Monthly means for the zonal wind component of the interpolated ERS-1 scatterometer data (top); for the initial guess, or ECMWF, fields (middle); and for the 5-day bin-averaged ERS-1 wind (bottom).

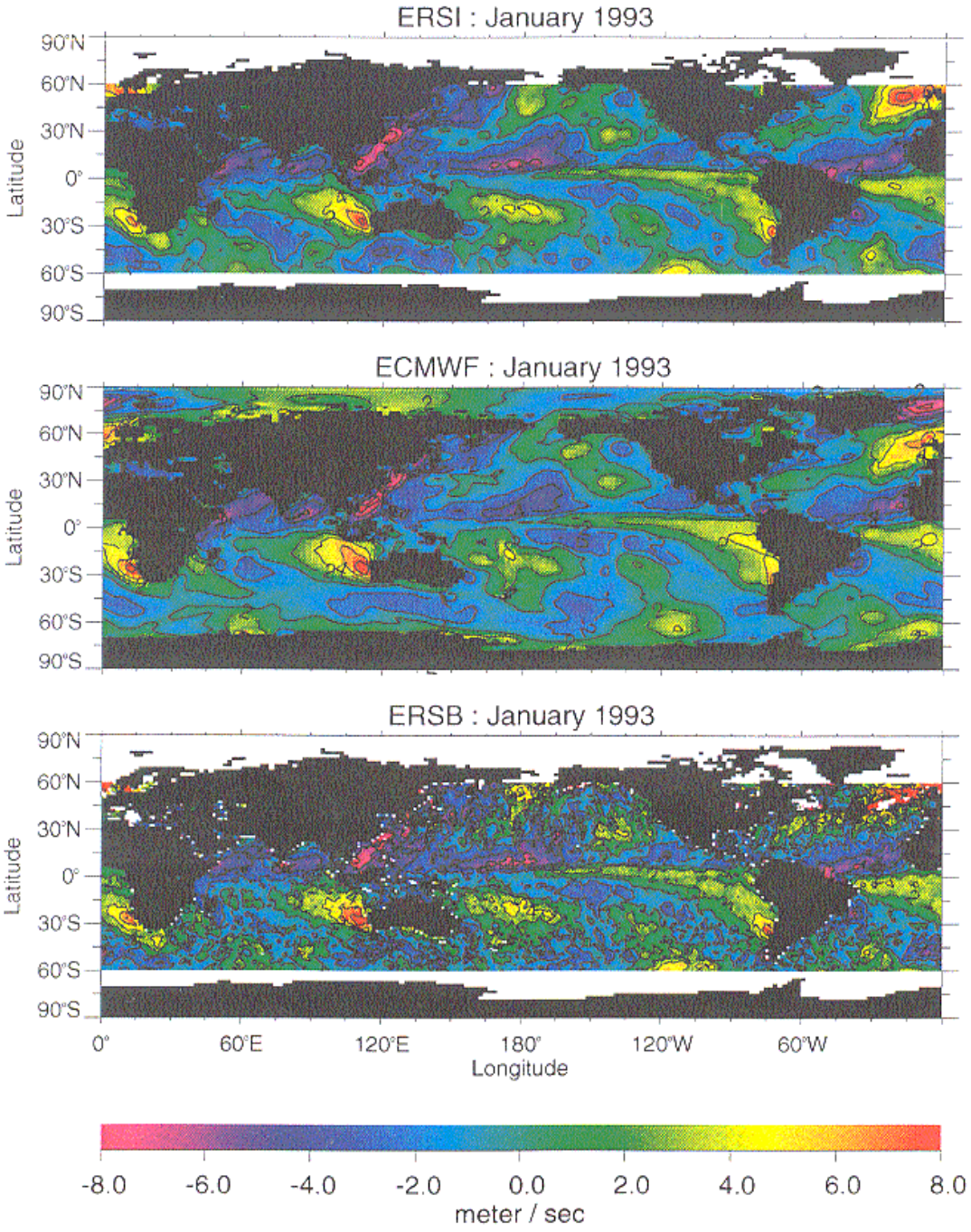

Fig.3b. Monthly means for the meridional wind component of the interpolated ERS-1 scatterometer data (top); for the initial guess, or ECMWF, fields (middle); and for the 5-day bin-averaged ERS-1 wind (bottom).

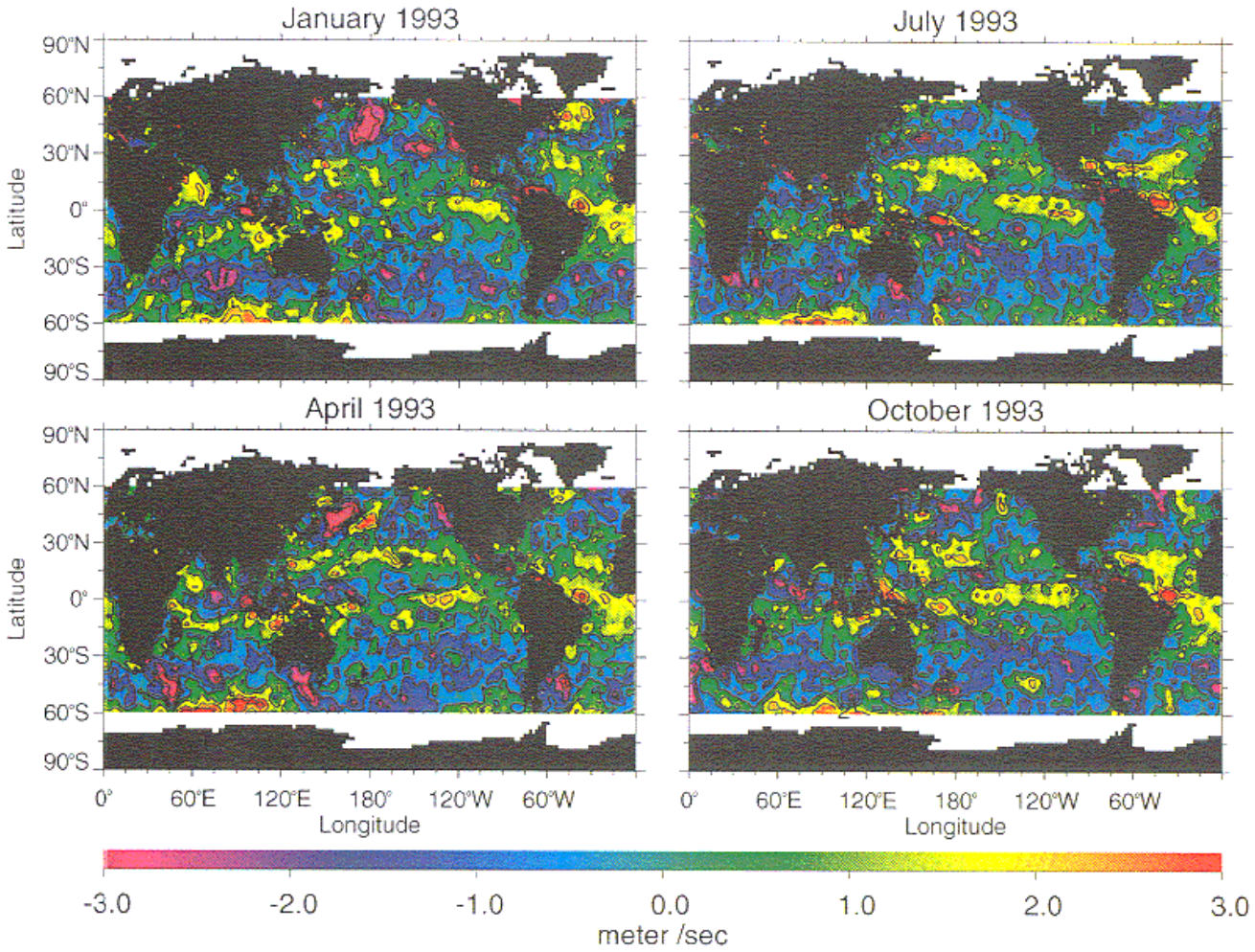

Fig.4a. Mean differences between the interpolated ERS-1 wind fields and the ECMWF wind fields for the zonal component for four typical months (January, April, July and October of 1993).

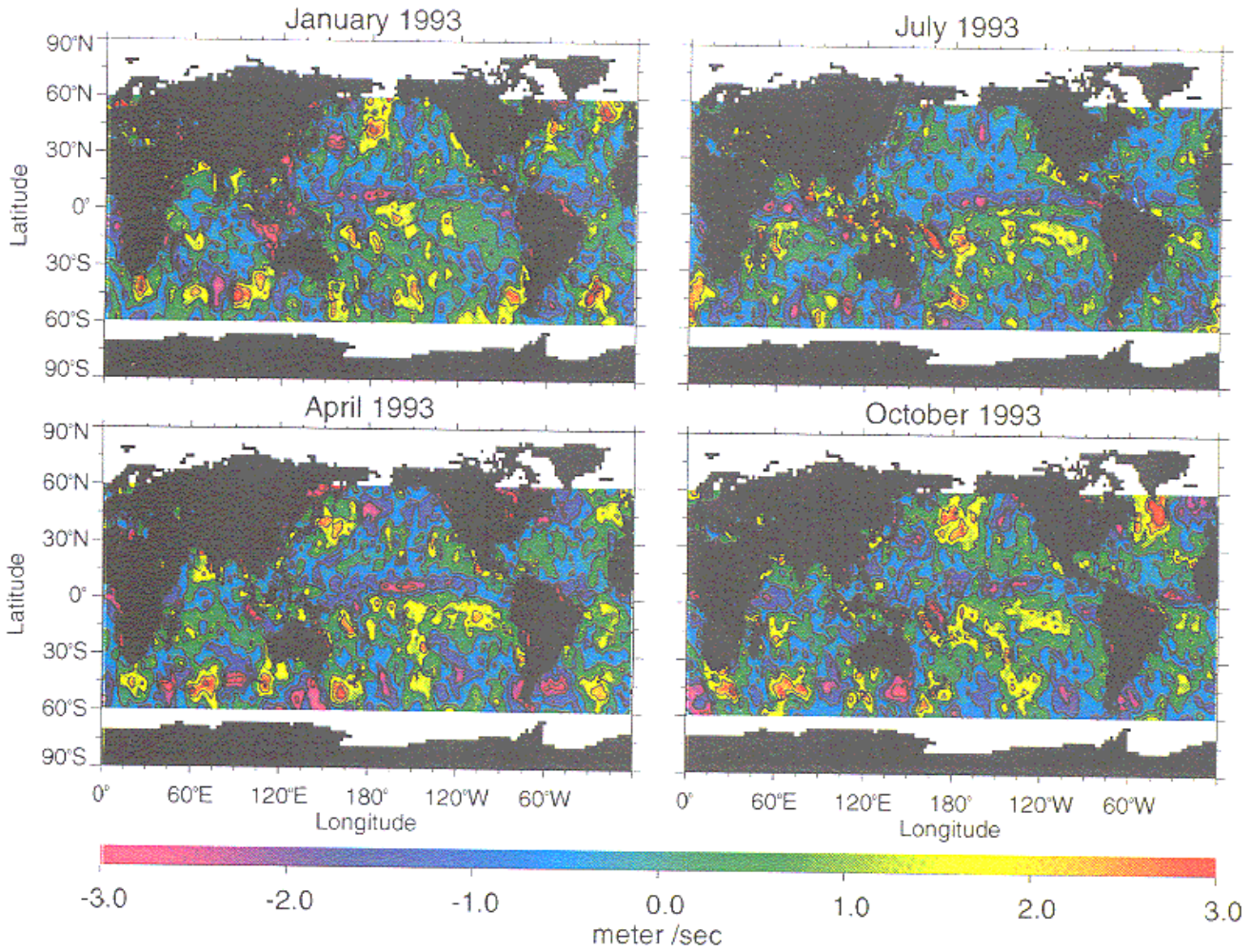

Fig.4b. Mean differences between the interpolated ERS-1 wind fields and the ECMWF wind fields for the meridional component for four typical months (January, April, July and October of 1993).

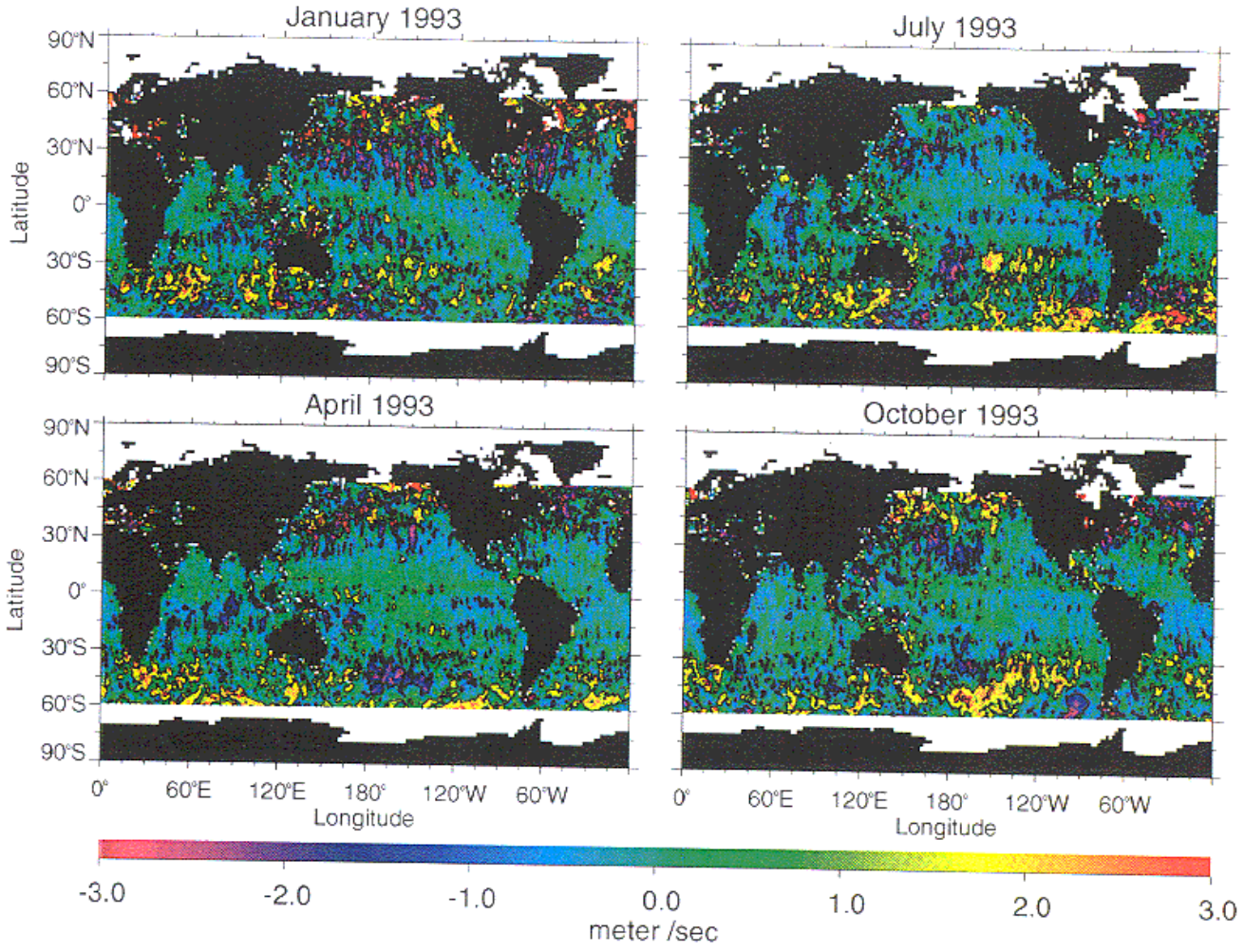

Fig.5a. Mean differences between the interpolated ERS-1 wind fields and the ERS-1 bin-averaged data for the zonal component for four typical months (January, April, July and October of 1993).

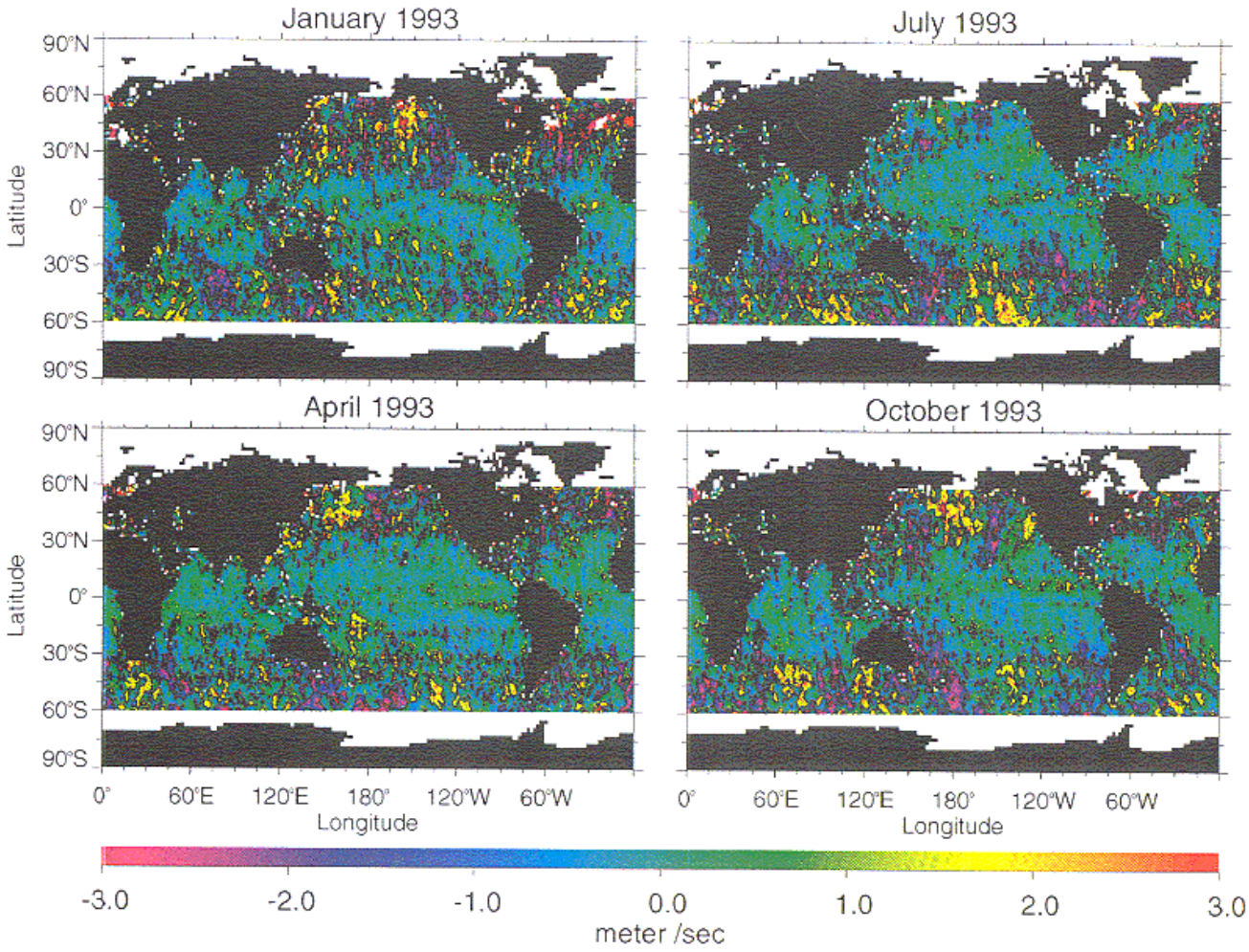

Fig.5b. Mean differences between the interpolated ERS-1 wind fields and the ERS-1 bin-averaged data for the meridional component for four typical months (January, April, July and October of 1993).

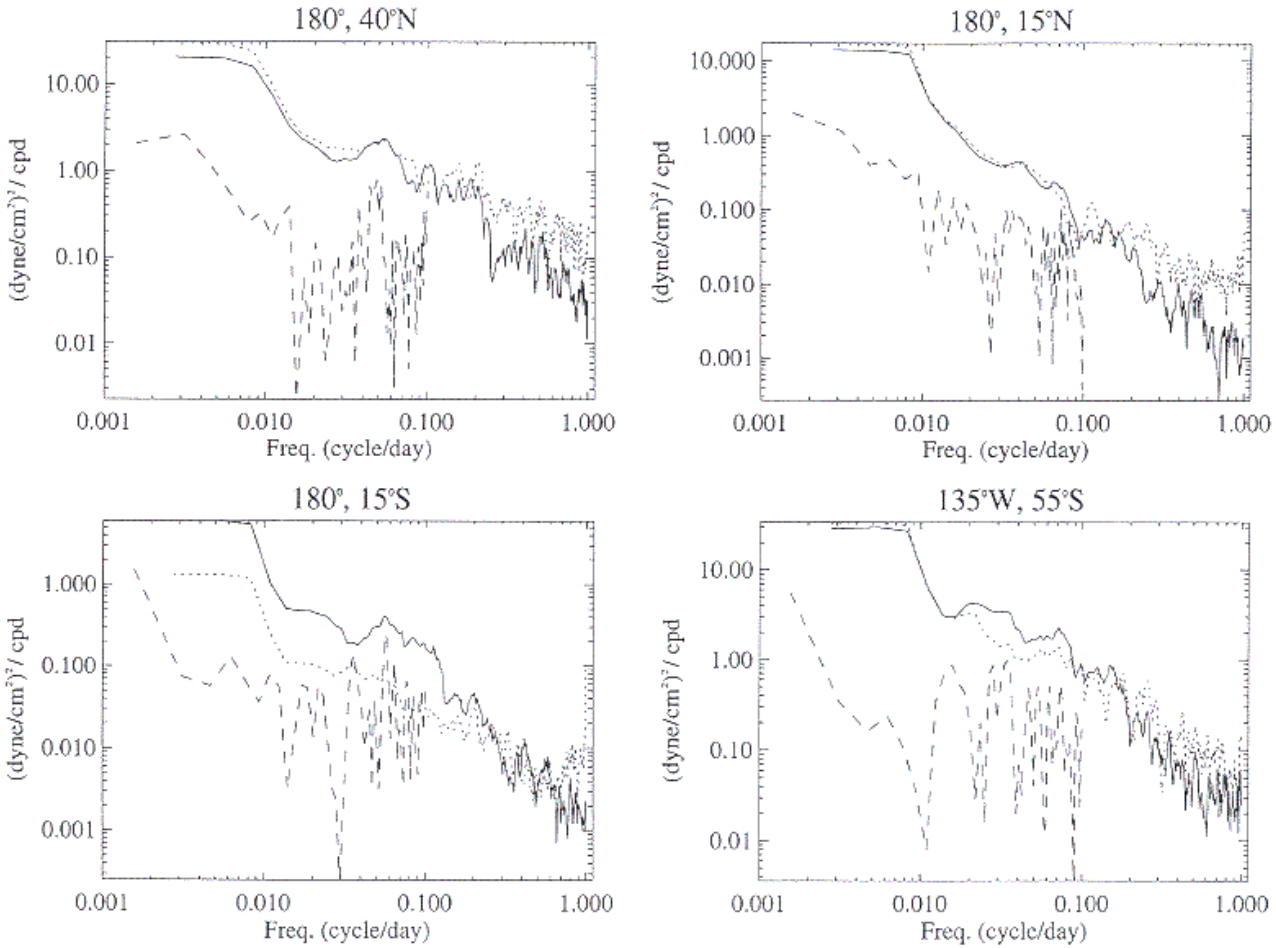

Fig.6a. Power spectra for three wind data sets: ERS-1 interpolated (solid), ECMWF (dotted) and ERS-1 bin-averaged (dashed) at four typical locations in the Pacific: (180°, 40°N), (180°, 15°N), (180°, 15°S) and (135°W, 55°S), for zonal wind stress.

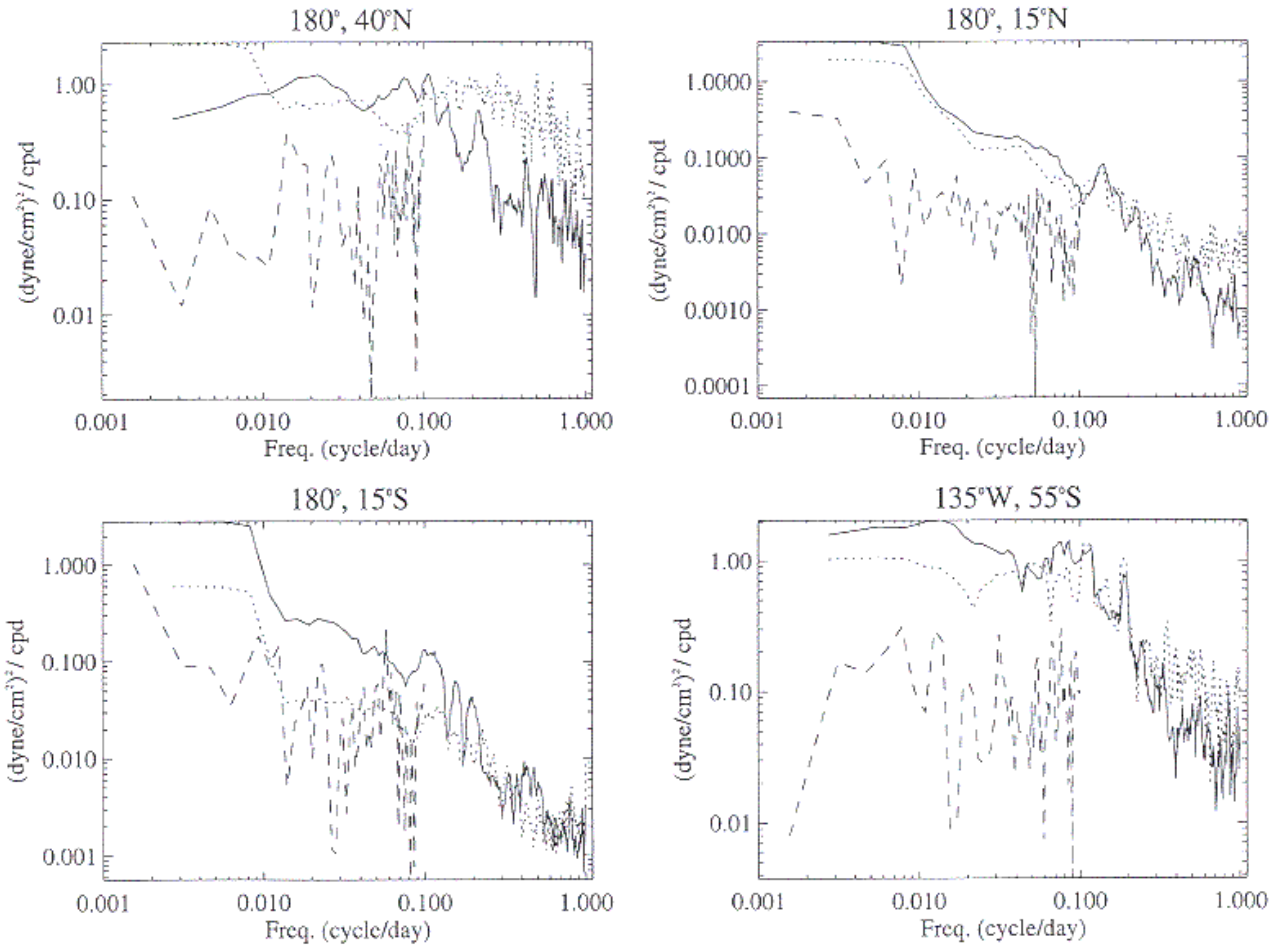

Fig.6b. Power spectra for three wind data sets: ERS-1 interpolated (solid), ECMWF (dotted) and ERS-1 bin-averaged (dashed) at four typical locations in the Pacific: (180°, 40°N), (180°, 15°N), (180°, 15°S) and (135°W, 55°S) for meridional wind stress.